Dynamics of Solar Coronal Eruptions

Bojan Vršnak

Hvar Observatory, Zagreb, Croatia

Short title: DYNAMICS OF SOLAR CORONAL ERUPTIONS

Abstract.

The kinematics of 87 solar eruptive events (flare-sprays, eruptive prominences and coronal transients) observed above the solar limb are studied. The data reveal a clear statistical trend for the highest measured value of the acceleration to be lower in the events taking place at a larger radial distance. The majority of events (84%) show a phase of exponential-like growth of the velocity. The growth rate decreases with the height at which this regime sets in. A phase of constant acceleration was found only in 11% of cases. In the post-acceleration phase a constant velocity regime was found in 57% of events. A considerable number of eruptions (32%) exposed a deceleration, most often showing an exponential-like decay of the velocity. The related theoretical models are confronted with the observations and the implications are discussed.

1. Introduction

Various forms of mass ejecta are observed in the solar atmosphere. Most generally, ejection events can be classified into two categories. In phenomena such as spicules, surges, X-ray jets, the plasma is ejected along the magnetic field lines, i.e. the trajectories are more or less controlled by stable magnetic field structures [*Shibata et al.,* 1994; *Tandberg-Hanssen,* 1995]. On the other hand, there are events such as eruptive prominences, sprays, loop or halo coronal mass ejections etc., which can be described as disruptions of unstable magnetic structures [*Vršnak et al.,* 1991; *Chen et al,* 1997; *Dere et al,* 1999].

The events belonging to the second category are usually interpreted as eruptions of destabilized magnetic flux tubes or magnetic arcades [*Vršnak et al.,* 1988; *Chen,* 1989; *Vršnak,* 1990; *Rust and Kumar,* 1994; *Chen,* 1996; *Filippov,* 1998]. They develop at various spatial and time scales, showing a wide range of velocities and accelerations [*Tandberg-Hanssen,* 1995]. Frequently, the erupting structures exhibit helical patterns revealing a previously hidden magnetic rope topology [*Vršnak* , 1992].

It seems that there are basically two types of eruptions from the kinematical point of view [*Tandberg-Hanssen et al.,* 1980]. Most of the events first show a phase of slow ascending motion which can be described as an evolution through a series of equilibrium states. At some point, the ascending object undergoes a fast acceleration. Typical events of this kind are eruptive prominences [*Tandberg-Hanssen,* 1995]. In the other kind of events, the phase of slow ascending motion is not prominent: the acceleration onset is abrupt and the eruption starts at very low heights, sometimes not more than several thousand kilometers [*Tandberg-Hanssen et al.,* 1980]. Such events are usually called sprays [*Tandberg-Hanssen,* 1995]. Very often they appear in emission in chromospheric spectral lines on the solar disc, and then they are called the flare-sprays. Let us note that in some classifications, an event has to achieve the escape velocity to be classified as a spray. Here, this demand will not be taken into accout.

Analogously, [*MacQeen and Fisher,* 1983] found in a sample of 12 events that flare related eruptions are fastly accelerated below the occulting disc of Mauna Loa Observatoty ($1.2R_{\odot}$) whereas the non-flare eruptions show a much weaker acceleration that is prolonged to larger heights.

Investigations of the kinematics of eruptions and studies of their helical morphology provide an important insight into the nature of eruptive processes [*Vršnak* , 1998]. Although observations of a large number of eruptive events were reported in past decades, detailed and systematic analyses of the kinematics were performed only occasionally, most often as a part of studies considering other problems ([*Gosling et al.,* 1976; *Tandberg-Hanssen et al.,* 1980; *Kahler et al.,* 1988; *Rompolt,* 1990; *MacQeen and Fisher,* 1983; *Sheeley et al.,* 1997]). Here, the kinematics of a number of events is studied systematically to investigate the most basic properties of solar coronal eruptions.

2. The Data

In this paper only the events rooted close to the solar limb are analysed. Several sources of data are used. They include Hvar Observatory Hα filtergrams and Skylab and SOHO coronographic images. This set is supplemented by a number of events studied previously by various authors (see Table 1). In some of these cases an additional analysis of the reported raw data and/or results was performed: e.g. the reported height-versus-time graphs were used to obtain the velocity-versus-time, velocity-versus-height graphs etc. In some cases the motion of the erupting feature was measured directly from the images exhibited in the considered report.

Out of 87 analysed events, 48 are white light coronal transients (CT), 31 are eruptive prominences (EP) and 8 are flare-sprays (FS). In Table 1 the events suitable for a detailed study of kinematics are listed. In the first two columns the event labels and the dates are given, respectively. The asterisk in the first column depicts the events for which only the graphical and/or numerical data from other sources (cited in the last column) were available. In the third column the class of the event is given. The events observed by coronographs (CTs) are divided into two subclasses: CAV denotes the cavity and CT denotes the bright frontal rim. Table 1

In most of the cases the basic information was the position (given either as the height h, or as the normalized radial distance from the solar center $R/R_\odot$) represented as a function of time t. In the case of CT and CAV events the height of the upper edge of the feature was measured (denoted as e.g. CAV-top in Table 1). Most of the studied eruptive prominences were shaped as arcs of a given width. In such cases the height of the upper and the lower edge of the arc was measured at its summit to determine the height of the mid-point, i.e. the height of the prominence axis (see e.g. [*Vršnak et al.,* 1997]). These cases are denoted as EP-mid in Table 1. When this procedure was not possible, or the data were taken from other sources, the height of the top of the erupting feature was used (denoted as EP-top). In FS events the erupting feature frequently does not exhibit clearly the arc structure and/or the lower edge of the arc is not well defined. So again the highest point of FS was measured (denoted as FS-top).

Let us stress that only in three cases different structural parts of the eruption were measured. In the event of December 19, 1973 the motion of the 3-part structure was followed – the prominence, the cavity and the bright frontal rim – whereas in the events of April 4, 1992, and April 30, 1992 the measurements of the prominence and the top of the cavity were available (Nos. 33/34, 36/37 and 17-19 in Table 1, respectively).

The smoothed $h(t)$ curves were used to evaluate the velocities (v) and accelerationons (a) and then the kinematical quantities h, v and a were represented in various forms of graphs in order to establish the functional dependences relating them. Usually the $v(t)$ and $v(h)$ graphs were considered, whereas the $a(t)$, $a(h)$ and $a(v)$ graphs were used only if the data were accurate enough. Finally let us note that in some cases, when the data were taken from other studies, only $v(h)$ or $\Delta h(t)$ relations were available.

There are several sources of errors in estimating the height of an eruptive feature. A mass loss and density decrease cause fading of its structural elements. In the case of Hα observations the traced feature can attain large radial velocity and can 'escape' from the filter band-pass due to the Doppler effect, or the plasma can be heated, also causing fading in Hα. On the other hand, particular structural elements can be additionally accelerated by some internal process and can show considerably higher velocities than the overall structure (see e.g. [*Rušin and Rybansky* 1982]). Finally, one has to take into account the projection effects, i.e. the velocity and the acceleration are measured only in the plane of sky.

The errors of the height measurements reflect in errors of v and a, becoming larger as succesive derivatives are taken. The errors of the acceleration estimates in the studied events are usually between 20% and 30% but can be larger than 60% and sometimes lower than 10% (see Table 1).

3. Kinematical Forms

In Figure 1 several examples of different observed kinematical forms are shown. Figure 1

Let us stress that the best examples are exhibited, so that error bars are smaller than the symbols used. In each case the $h(t)$ graph is exhibited in the left hand side column to show the most basic representation of the motion. The graphs presented in the middle and the right hand side column are chosen in such a way to reveal most clearly a particular kinematical form.

In Figure 1a an event whose development can be represented by an exponential-like growth is shown. The motion where the height increases exponentially after the moment t_0, when the erupting feature is located at the height h_0, can be described as:

$$h(t) = h_0 e^{\omega(t-t_0)} \ , \tag{1}$$

implying:

$$\dot{h} \equiv v = \omega h \qquad \text{and} \qquad \ddot{h} \equiv a = \omega^2 h \ . \tag{2}$$

The events in which such a kinematical form is prominent during the acceleration phase are denoted further on by 'exp.'. This type of motion can be most easely recognized in the $v(h)$ graph since $v \propto h$, providing also a straightforward estimate of the growth rate $\omega = \Delta v/\Delta h$. Let us stress here that the events are classified as 'exp.' if an exponential fit to the data was reasonable. However, most of the data could be fitted at the comparable confidence level also by polynomial or various forms of power-law functions at least to a part of the $h(t)$ curves (see e.g. [*Kahler et al.,* 1988], [*Sheeley et al.,* 1997] or [*Hiei,* 1998]). So, it should be noted that the 'exp' events do not necessarily imply that the process of eruption is governed by a linear instability.

The prominence eruption exhibited in Figure 1a starts to grow exponentially after the prominence attained the height $h_0 \approx 30$ Mm (see the middle panel of Figure 1a). The pre-exponential phase is shown by small crosses, whereas the exponential-like phase is shown by larger crosses and the corresponding least square fit. In the right hand side panel of Figure 1a the $a(h)$ graph is presented, clearly reproducing Equation (2). From the presented fits in the middle and the right hand side graphs, one finds $\omega_v = \Delta v/\Delta h \approx 4.9\,10^{-3}\,\mathrm{s}^{-1}$ and $\omega_a = \sqrt{\Delta a/\Delta h} \approx \sqrt{29.65\,10^{-6}} = 5.4\,10^{-3}\,\mathrm{s}^{-1}$, respectively, i.e. $\omega_v \approx \omega_a$.

Figure 1b represents an event in which the acceleration phase is governed by a linear increase of velocity in time ($v \propto t$), i.e. by $a = const.$ Such behaviour is suggestive of an approximately constant driving force that dominates the gravity and viscous drag. The events of this kind will be denoted further on by '$a = const.$'.

The events for which it was possible to estimate the highest value of acceleration (a_m) and the associated height (h_m), or the values of ω and h_0, are listed in Table 1.

The mean values are given at the bottom of the table.

Figures 1c-1e show various types of motion observed after the main acceleration phase. In Figure 1c an example is exhibited where the acceleration slowly decreases, i.e. $\partial a/\partial t < 0$. Such cases will be denoted further on by '$a \searrow$'. The example exhibited in Figure 1c shows an exponential-like decrease of acceleration with the height (the data used for the least square fit are denoted by larger dots). This type of motion can be expected if the driving force decreases with height.

For the matter of generality, let us stress that $a \searrow$ can occur also if the driving force is not vanishing. Taking into account the viscous drag and using the simplest possible approximation $f_v = -\gamma v$, one can write for the acceleration:

$$\ddot{h} = f_{driv} - \gamma \dot{h} \ . \tag{3}$$

where f_{driv} is the driving force per unit mass. Equation (3) shows that even in the cases when f_{driv} is not decreasing (e.g. $f_{driv} \approx const.$ for a period of time) the acceleration $a = \ddot{h}$ decreases. This can happen if the driving force has a flat maximum and the attained velocity is already high.

It is hard to decide between the two possibilities on the basis of the observations analysed in this paper. However, the theoretical considerations (see Section 5) seem to favour the first one, i.e. the ceasing of driving force. In any case, the result is that the velocity becomes constant and the eruption enters into the $v = const.$ regime. An example of an eruption with a prominent '$v = const.$' phase is shown in Figure 1d.

In 14 cases a decrease of the velocity of eruption was observed in the late phases of the eruption, which implies $a < 0$. Such cases are denoted further on by '$v \searrow$'. The decrease is most often (11 cases) exponential-like. Such a behaviour can be expected if $f \to 0$ is assumed, and then Equation (3) becomes:

$$\dot{v} = -\gamma v\,, \tag{4}$$

and one finds $v = v_0 e^{-\gamma t}$, implying $v = v_0 - \gamma h$. An example of such a motion is shown in Figure 1e.

In all of the 11 cases which showed the exponential-like decrease of the velocity the values of γ were estimated. The mean value for five CT events amounts to $\gamma = (0.8 \pm 0.2)\,10^{-4}$ s^{-1} and for six EP+FS events $\gamma = (0.8 \pm 0.6)\,10^{-3}$ s^{-1}. The later value is consitent with the previously obtained values for lower corona ([*Vršnak et al.,* 1997] and references therein). The mean radial distance at which the decceleration was taking place amounts to $R/R_\odot = 7 \pm 3$ for CTs and $R/R_\odot = 1.23 \pm 0.10$ for EPs+FSs.

There are two points which should be stressed here. First, it should be noted that Equations (3) and (4) do not account for solar wind effects which become important at the radial distances of several $R_\odot$ [*Sheeley et al.,* 1997]. Furthermore, [*Cargill et al.,* 1996] found in an MHD numerical simulation that flux ropes experience drag that is quadratic in speed. Bearing in mind these two points, the value of γ obtained for CTs should be taken with caution.

The eruption presented in Figure 1f is a specific example showing in its late phase a very rapid deceleration before resting at an upper equilibrium position. In this event one finds first the slow pre-eruptive ascending motion (denoted as A in the middle panel of Figure 1f). Then, after $h_0 \approx 10000$ km was reached an exponential-like growth starts (phase B), lasting up to the height of $h \approx 20000$ km. A short $v \approx const.$ phase shows up (phase C) before the velocity suddenly starts to decrease (the acceleration becomes negative) at $h \approx 25000$ km. The velocity sharply drops (phase D) to become $v \approx 0$ after the eruption reached $h_{up} = 30000$ km. At the same time the acceleration also drops to $a \approx 0$.

In Table 2 the occurrence rate of different kinematical forms is shown separately for FS, EP and CT categories. During the main acceleration phase the events are classified to 'exp.' and '$a = const.$' types. The irregular motions that could not be classified are denoted by 'ir.'. The behaviour after the main acceleration phase is categorized as '$a \searrow$', '$v = const.$' and '$v \searrow$'. Table 2

The questionmark '?' in Table 2 denotes the cases where it was not possible to classify the kinematical form either because the phase was not observed or the observations do not allow a decision (e.g. the insufficient time or spatial resolution, etc.). A relatively large percentage of '?' cases in the early phases of CTs and late phases of FSs and EPs is caused by observational constraints. The acceleration phase of CT very often ends before CT rises over the occulting disc of the coronograph, whereas erupting features are too faint to be traced in the Hα observations in the post-acceleration phase.

When '?' cases are excluded one finds that an exponential-like growth of the eruption is the dominant kinematical form during the acceleration phase in all categories of the events. It was found in 84% of the observed eruptions. A constant acceleration phase showed up as a distinctive phase in only 11% of the events, similarly as a decrease of the acceleration at the end of the main acceleration phase.

A prominent '$v = const.$' form is found in the majority of CT events in the post-acceleration phase. About 2/3 of the studied CTs show such behaviour. In the case of Hα observations (i.e. considering FSs and EPs together) '$v = const.$' and '$v \searrow$' are equally represented in the studied sample.

4. Accelerations and Growth Rates

The acceleration was measured on the smoothed $v(t)$ curves. In Figure 2a the maximum value of the acceleration a_m is presented as a function of the height h_m at which it was measured, separately for FSs, EPs and CTs (see Table 1). The presented sample consists of 34 events for which it was possible to estimate the values of a_m and h_m. In other cases either the acceleration phase was not observed or the acceleration was still increasing at the end of observations, or the value of h_m was not available (in 22 cases taken from other studies the initial height was set to $h = 0$). In Table 3 the logarithmic mean values of a_m and h_m are presented ($\overline{a}_{log}$ and $\overline{h}_{log}$, respectively). The local value of the acceleration of gravity $g_m = g(h_m)$ is also given and one finds that the average a_m is comparable with g in EPs, it is several times higher in CTs and an order of magnitude higher in FSs.

Figure 2

Table 3

Let us consider the process of acceleration in more detail. The acceleration can be expressed as $a = f_{driv} - g - f_v$, where $g = 274(R_\odot/R)^2$ is the acceleration of gravity. Inspecting the values of $v_m = v(h_m)$ and a_m in all cases individually and taking into account the estimated values of γ at the corresponding haight range, it was found that

f_v can be neglected during the maximum acceleration in the majority of events. So, the maximum value of the driving force can be estimated as $f_m^{driv} \approx a_m + g_m$.

In Figure 2b the values of $f_m = a_m + g_m$ are shown as a function of $R/R_\odot$. The mean values for FSs, EPs and CTs are given at the bottom of Table 1 and the logarithmic means are given in Table 3. The graphs in Figures 2a and 2b clearly indicate a decrease of the average driving force with height. Note that the event error bars are smaller than the scatter of the data points. The empirical dependence found in Figure 2b can be expressed in the form:

$$f_m = 752 \left(\frac{R_m}{R_\odot} \right)^{-1.720} \quad . \tag{5}$$

Using an analogus graph showing $f_m(h_m)$ one would find:

$$f_m = 6716\, h_m^{-0.568} \ . \tag{6}$$

A large percentage of the events showed an exponential-like development (Table 1). For 38 cases (Table 1) it was possible to determine the growth rate $\omega = \Delta v / \Delta h$ (see Equations (1) and (2)) and the height h_0 at which the eruption entered this regime. In Figure 3 the measured values of ω are presented as a function of h_0 separately for FSs, EPs and CTs. Note that the error bars are again smaller than the scatter of data points. The least square fit for the displayed events gives: Figure 3

$$\omega = 23.5\, h_0^{-0.692} \ , \tag{7}$$

where ω is expressed in 10^{-3} s^{-1} and h in Mm. If the data were shown in the $\omega(R/R_\odot)$

graph one would find:

$$\omega = 2.0 \left(\frac{R_m}{R_\odot}\right)^{-2.487} . \tag{8}$$

At the bottom of Table 1 the mean values of ω and h_0 are shown for FSs, EPs and CTs separately, whereas in Table 3 the logarithmic mean values are given.

5. Conclusions and Discussion

In the majority of the studied cases the process of eruption can be divided into three phases: 1) slow ascending motion, 2) acceleration phase, 3) post-acceleration phase. The first phase is characterized by velocities in the order of 10 $\mathrm{km\,s^{-1}}$ and can be represented as an evolution through a series of quasi-equilibrium states. This phase is most prominent in EPs. FSs also show this phase (see Figures 1a and 1f) but of a much shorter duration.

The acceleration begins at different heights for FSs, EPs and CTs. For FSs the heights are in the order of 10 Mm, whereas EPs start accelerating most often at heights between several tens of Mm and 100 Mm. Bearing in mind that in most of CTs the acceleration happened below the occulting disc of the coronograph ('?' cases in Table 1) and inspecting Figure 2 it can be concluded that the majority of eruptions show an acceleration maximum below $R/R_\odot \approx 4$. The main acceleration phase in all categories of events is most often characterized by an exponential-like increase of the velocity.

The values of a_m and $f_m = a_m + g_m$ are smaller for objects accelerating at larger heights. Similarly, faster growth rates are found at lower heights. Bearing in mind that a CME events usually show 3-part structure – the prominence, the cavity and the bright frontal rim – an interesting question arises: do all three elements show the same growth rate, or the rates differ, maybe showing a tendency similar to the one revealed by Figure 3. Usually, the frontal rim is faster than the prominence (see e.g. [*Illing and Hundhausen,* 1986]), and in the case that the growth rate is slower than for the prominence (Figure 3 suggestive) it should be compensated by a sufficiently longer phase of growth.

Unfortunatelly, only in three events from the studied sample (cases Nos. 17-19, Nos. 33/34 and Nos. 36/37) it was possible to determine characteristics of motion of the associated parts of eruptions (in Figures 2 and 3 the associated data points are connected by dashed lines). Inspecting Table 1 one finds that in the case of the event 17-19 the prominence showed a faster growth rate then CAV and CT ($\omega_{EP-top} \approx 2\omega_{CAV-top}$ and $\omega_{CAV-top} \approx \omega_{CT-top}$) and that the difference is significantly higher than the error estimates. However, CAV and CT growth was lasting longer, leading to higher accelerations and final velocities than for EP. The exponential-like growth of CT/CAV covered the height range of about 1500 Mm, whereas in the EP case it embraced less than 500 Mm. The resulting velocities were 300 and 120 km s^{-1}, and the accelerations 35 and 5 m s^{-2}, respectively.

On the other hand, events No. 33/34 and No. 36/37 show a different tendency: CAV-top shows a significantly faster growth and a stronger acceleration than EP in both events. In the case No. 33/34 the exponential growth of CAV covered considerably smaller height range then of EP (about 150 Mm and 400 Mm, respectively). Due to this difference which compensated the faster growth rate the attained velocities were about the same (≈150 $\mathrm{km\,s^{-1}}$). In the event No. 36/37 the exponential-like growth of EP and CAV covered a comparable height range (about 600 Mm and 400 Mm, respectively) so CAV attained the velocity of 300 $\mathrm{km\,s^{-1}}$ and EP only 150 $\mathrm{km\,s^{-1}}$.

All three events indicate that the motion of various elements of an erupting structure is governed by different time profiles. The events 33/34 and 36/37 behave as predicted in the model by [*Chen,* 1996] – the prominence component located below the erupting flux tube axis should be more inert (due to a higher mass density ρ) than the less dense cavity above. Furthermore, it should be noted that although the accelerations a_m are considerably different, the values of $f_m = a_m + g_m$ in the three considered events are quite similar for different parts of the structure (see Figure 2b). This, as well as the described behaviour of the event No. 17-19, indicates that the volume force ρf is stronger in the prominence part of the structure.

These three particular examples call for a coordinated Hα and coronographic observations and a detailed analysis of a larger number of the events showing 3-part structure. Only then, more reliable and more general conclusions about the behaviour of driving force in different parts of erupting structures could be drawn.

The graphs shown in Figures 2 and 3 indicate a possible distinction between the FS, EP, and CT categories since they are clustered in different regions of these graphs. The distribution of events in Figure 3 shows a gap between FS events and EP/CT events. However, let us stress that larger samples should be analysed to draw any definite conlusion, since the gap could be caused by observational effects. For example, removing the events Nos. 24, 25, 27, 28 and 29 (denoted by black triangles in Figure 3) which are five events taken from [*MacQeen and Fisher,* 1983] one would get also a gap between EP and CT events. This gap would be obviously artificial, appearing only because of lack of the observations in the range of heights covered by Mauna Loa Observatory (1.2-2.4 $R_\odot$). The gap between FS and EP events could be a similar artefact. FSs are bright in Hα and can be detected by observations suited for solar disc studies (a narow filter band-pass, short 'exposure-times') unlike EPs. The later are usually observed above the limb using broader band-pass filters and longer 'exposures'. So it is possible (although not likely) that the events which would be bridging the gap between FSs and EPs might have such characteristics that are making them difficult to be detected by either kind of observations.

At first glance, the gap between FSs and EPs is suggestive of the results presented by [*MacQeen and Fisher,* 1983] who concluded that flare related CMEs are basically different from the non-flare CMEs since the former are accelerated at much lower heights ($R/R_\odot < 1.2$) and at much faster rate than the later ones. However, the classification to FS, EP and CT categories used in this paper is based primarily on kinematical and morphological characteristcs of the events, and not on the flare-association as in [*MacQeen and Fisher,* 1983]. So, classifying an eruption into EP or CT category does not imply that it was not associated with a flare. In particular, the events No. 43, 44, 45 were related to powerful, long duration X-class flares and they were still accelerating at the distances beyond $R/R_\odot = 3$ (see Table 1), thus opposing the conclusion by [*MacQeen and Fisher,* 1983]. Since it was not possible to establish a reliable flare-association for all of the events listed in Table 1 (in a number of cases only the time elapsed after the beginning of eruption was given in the data source) the fraction of flare-related eruptions that are accelerating at $R/R_\odot > 1.2$ could be even larger.

Finally, it should be noted that even if the gap between FS and EP/CT categories is not an artefact, the correlations revealed in Figures 2 and 3 indicate that forces driving the eruptions of both kind follow a common scaling law. Furthermore, the events of all three categories may, or may not achieve the escape velocity. So, from the kinematical point of view, a distinction between these categories should be made primarily on the basis of the values of ω, h_0, a_m and h_m: the acceleration of an average FS is an order of magnitude higher than in the case of EP/CT, it grows at an order of magnitude faster rate and attains maximum at least at an order of magnitude lower height.

The observed kinematical forms summarized in Figure 1 can be directly related to the models proposed by [*Chen,* 1989] and [*Vršnak,* 1990] (see also [*Chen,* 1996] and [*Vršnak et al.,* 1993], respectively). In the former model the eruption is a response to an injection of the poloidal magnetic flux into the rope, and in the later case the initially stable, slowly evolving magnetic structure erupts due to a loss of equilibrium. Both models treat forces acting in a curved (toroidal-like) flux rope anchored at both ends in the dense photosphere.

The interplay between different Lorentz force contributions and the gravity in both models predicts an exponential-like growth of acceleration in early stages of eruption (see Table 2 and Figure 1a). The acceleration attains maximum at some height depending on the initial internal configuration and the overall geometry of the rope. This phase can be identified as a phase of $a \approx const.$ (Figure 1b).

In both models the driving force ceases at heights above few $R_\odot$. The acceleration decreases (see Figure 1c) and the eruption enters into a constant velocity regime (Figure 1d). Such behaviour is fairly consistent with Figure 2a showing that most of events attain maximum acceleration below $R/R_\odot \approx 4$.

In addition to the mentioned forces the Chen's model takes into account the viscous drag (quadratic in velocity), whereas the Vršnak's model allows the reconnection below the erupting flux rope (like in two-ribbon flares) which is in a way a late phase counterpart of the Chen's initial poloidal flux input. Furthermore, both models take into account the mass loss and the transport of the twist into expanded summit of the rope. The transport of twist, mass loss and the reconnection below the rope tend to prolong the acceleration. These effects might explain the events in Figure 2a which show the maximum acceleration beyond $R/R_\odot \approx 4$. On the other hand, the drag tends to slow down the motion (see Figure 1e). Chen's model predicts that due to the drag the CMEs that attained velocity higher than the solar wind should be decelerated, whereas the CMEs that are slower than solar wind should be additionally accelerated (see [*Gopalswamy et al.,* 2000]). Let us stress that only in the case of the event No. 40 an acceleration by the solar wind could be possible since the eruption velocity was about 200 $\mathrm{km\,s^{-1}}$ at the radial distance $R/R_\odot \approx 7$ which is comparable with the wind speed at this distances [*Sheeley et al.,* 1997]. In all other events the eruption velocity was considerably higher than the wind speed at the corresponding radial distance.

In the low corona events, where solar wind effects can be neglected, ceasing of the driving force at some height and the action of viscous drag can cause the termination of motion at an upper equilibrium position (see Figure 1f). Let us note that Vršnak's model predicts oscillations about the upper equilibrium for particular initial magnetic field configurations if the eigenmode frequency there is higher than the value of γ. Such oscillations were observed by [*Vršnak et al.,* 1990].

Finally, let us note that both models predict that the growth rate of eruption can be expressed as:

$$\omega = \frac{v_A}{L}\sqrt{\psi(X,Z)}\ , \tag{9}$$

where v_A is the Alfvén velocity, L is the length of the loop and $\psi(X,Z) \lesssim 1$ is a function of the magnetic flux rope twist X, and the geometrical shape of the loop (expressed by the ratio Z of the initial height and the footpoint separation). Since the length of the loop L is related to its height, it can be expected that the growth rate decreases with the height as found in Figure 3.

References

Anzer, U., Can Coronal Loop Transients be Driven Magnetically? *Solar Phys., 57,* 111-118, 1978.

Cargill, P. J., J. Chen, D. S. Spicer, and S. T. Zalesak, Magnetohydrodynamic Simulations of the Motion of Magnetic Flux Tubes through a Magnetized Plasma *J. Geophys. Res., , 101,* 4855-4870, 1996.

Chen, J., Effects of Toroidal Forces in Current Loops Embedded in a Background Plasma, *Astrophys. J., 338,* 453-470, 1989.

Chen, J., Theory of Prominence Eruption and Propagation: Interplanetary Consequences, *J. Geophys. Res., 101,* 27,499-27,519, 1996.

Chen, J., R. A. Howard, G. E. Brueckner, R. Santoro, J. Krall, S. E. Paswaters, O. C. St. Cyr, R. Schwenn, P. Lamy, and G. M. Simnett, Evidence of an Erupting Magnetic Flux Rope: LASCO Coronal Mass Ejection of 1997 April 13, *Astrophys. J., 490,* L191-L194, 1997.

Dere, K. P., G. E. Brueckner, R. A. Howard, and D. J. Michels, LASCO and EIT Observations of Helical Structure in Coronal Mass Ejections, *Astrophys. J., 516,* 465-474, 1999.

Dryer, M., and 23 coauthors, The Solar Minimum Active Region 7978, *Solar Phys., 181,* 159-183, 1998.

Engvold, O., and B. M. Rustad, An Eruptive Prominence of June 10, 1973, *Solar Phys., 35,* 409-417, 1976.

Filippov, B. P., Causes and Effects of Filament Eruptions, in *New Perspectives in Solar Prominences,* edited by D. Webb, D. Rust and B. Schmieder, pp. 342-349, ASP Conf. Series *150*, San Francisco, California, 1998.

Godoli, G., M. L. Sturiale and S. Torrisi, Special Solar Events Observed at Catania Astrophysical Observatory, in *Memorie della Societa Astronomica Italiana., 38,* pp. 6-13, Osservatorio Astrofisico di Catania, Catania, Italy, 1967.

Gopalswamy, N., A. Lara, R. P. Lepping, M. L. Kaiser, D. Berdichevsky, and O. C. St. Cyr, Interplanetary Acceleration of Coronal Mass Ejections, *Geophys. Res. Lett., 27,* 145-148.

Gosling, J. T., E. Hildner, R. M. MacQueen, R. H. Munro, A. I. Poland, and C. L. Ross, The Speeds of Coronal Mass Ejections, *Solar Phys., 48,* 389-397, 1976.

Hiei, E., Prominence Disappearance Related to CMEs, in *New Perspectives in Solar Prominences,* edited by D. Webb, D. Rust and B. Schmieder, pp. 380-383, ASP Conf. Series *150*, San Francisco, California, 1998.

Illing, R. M. and A. J. Hundhausen, Disruption of Coronal Streamer by an Eruptive Prominence and Coronal Mass Ejection, *J. Geophys. Res., 91,* (A10), 10951-10960, 1986.

Kahler, S. W., R. L. Moore, S. R. Kane, and H. Zirin., Filament Eruptions and the Impulsive Phase of Solar Flares, *Astrophys. J., 328,* 824-829, 1989.

Lenža, L., Hα Observations of the Dual Eruptive Prominence of June 29, 1994, in *New Perspectives in Solar Prominences,* edited by D. Webb, D. Rust and B. Schmieder, pp. 323-325, ASP Conf. Series *150*, San Francisco, California, 1998.

Machado, M. E., Analysis of Two Active Prominences, *Solar Phys., 23,* 353-359, 1972.

MacQueen, R. M., and R. R. Fisher, The Kinematics of Solar Inner Coronal Transients, *Solar Phys., 89,* 89-102, 1983.

Rybansky, M., Eruptive Prominence of 3 May 1971, *Bull. Astron. Inst. Czechosl., 22,* 380-382, 1971.

Rybansky, M., and G. Noony, Eruptive Prominence of September 15, 1989, *Bull. Astron. Inst. Czechosl., 41,* 269-270, 1990.

Rompolt, B., Small Scale Structure and Dynamics of Prominences, *Hvar Obs. Bull., 14,* 37-102, 1990.

Rust, D. M. and A. Kumar, Helical Magnetic Fields in Filaments, *Solar Phys., 155,* 69-97, 1994.

Rušin V and M. Rybansky, Eruptive Prominence of August 18, 1990, *Bull. Astron. Inst. Czechosl., 33,* 219-229, 1982.

Sakurai, T., Magnetohydrodynamic Interpretation of the Motion of Prominences, *Publ. Astron. Soc. Japan, 28,* 177-198, 1976.

Schmahl, E. and E. Hildner, Coronal Mass Ejections - Kinematics of the 19 December 1973 event, *Solar Phys., 55,* 473-490, 1977.

Sheely, Yr. N.R., Y.-M. Wang, S. H. Hawley, G. E. Brueckner, K. P. Dere, R. A. Howard, M. J. Koomen, C. M. Korendyke, D. J. Michels, S. E. Paswaters, D. G. Socker, O. C. St. Syr, D. Wang, P. L. Lamy, A. Llebaria, R. Schwenn, G. M. Simnett, S. Plunkett, and D. A. Biesecker, Measurements of Flow Speeds in the Corona Between 2 and 30 $R_{\odot}$, *Astrophys. J., 484,* 472-478, 1997.

Shibata, K., T. Yokoyama, and M. Shimojo, Coronal X-ray Jets, in *Proceedings of Kofu Symposium,* edited by S. Enome and T. Hirayama, pp. 75-78, Nobeyama Radio Observatory, NAOJ, Nagano, Japan, 1994.

Tandberg-Hanssen, E. *The Nature of Solar Prominences,* Kluwer Academic Publishers, Dordrecht, The Netherlands, 1995.

Tandberg-Hanssen E., S. F. Martin, and R. T. Hansen, Dynamics of Flare Sprays, *Solar Phys., 65,* 357-368, 1980.

Vršnak, B., Eruptive Instability of Cylindrical Prominences, *Solar Phys., 129,* 295-312, 1990.

Vršnak, B., Magnetic Structure of Solar Prominences, *Annales Geophys., 10,* 344-353, 1992.

Vršnak, B., Prominence Eruptions, in *New Perspectives in Solar Prominences,* edited by D. Webb, D. Rust and B. Schmieder, pp. 302-309, ASP Conf. Series *150*, San Francisco, California, 1998.

Vršnak, B., V. Ruždjak, R. Brajša, and A. Džubur, Structure and Stability of Prominences with Helical Structure, *Solar Phys., 116,* 45-60, 1988.

Vršnak, B., V. Ruždjak, R. Brajša, and F. Zloch, Oscillatory Motions in an Active Prominence, *Solar Phys., 127,* 119-128, 1990.

Vršnak, B., V. Ruždjak, and B. Rompolt, Stability of Prominences Exposing Helical-Like Patterns, *Solar Phys., 136,* 151-167, 1991.

Vršnak, B., V. Ruždjak, B. Rompolt, D. Roša, and P. Zlobec, Kinematics and Evolution of Twist in the Eruptive Prominence of August 18, 1980, *Solar Phys., 146,* 147-162, 1993.

B. Vršnak, Hvar Observatory Faculty of Geodesy, Zagreb University, Kačićeva 26, HR-10000 Zagreb, Croatia. (e-mail: bvrsnak@geodet.geof.hr)

Received ?????; revised ?????; accepted ?????.

To appear in the *Journal of Geophysical Research*, 2000.

Figure 1. Observed kinematical forms: squares represent the height, crosses the velocity and circles the acceleration. Left: $h(t)$ graphs. Middle and right: the graphs exposing most directly a given kinematical form. The measurements used for the least square fits are denoted by larger symbols. a) FS of September 5, 1973 – exponential-like growth. b) EP of December 19, 1973 – prominent $a \approx const.$ phase. c) EP of April 30, 1974 – an exponential-like decrease of acceleration with height. d) EP of July 19, 1975 – prominent $v = const.$ phase. e) CT of June 16, 1998 – deceleration: an exponential-like decrease of the velocity. f) FS of August 3, 1970 – the eruption approaching an upper equilibrium position. In this event different phases of the eruption are denoted as: A – slow ascending motion; B – the exp. phase; C – the $v = const.$ phase; D – the deceleration phase.

Figure 2. a) The maximum acceleration a_m versus the height h at which it was measured. b) The dependence of $f_m = a_m + g_m$ on the radial distance. Squares represent FSs, circles EPs and triangles CTs. The least square fits are drawn by thick lines and the functions $g(h)$ and $g(R/R_\odot)$ by the thin lines. The data points belonging to the same event are connected by the dashed line.

Figure 3. The growth rate $\omega = \Delta v/\Delta h$ versus the height at which the 'exp.' phase had started. Squares represent FSs, circles EPs and triangles CTs (black triangles are the 'Mauna Loa events' taken from [*MacQeen and Fisher,* 1983]). The best fit is drawn by the full line. The data points belonging to the same event are connected by the dashed line. In the inset the logarithmic mean values and standard deviations are shown.

Table 1. List of Events

Displayed in Figures 2 and 3

No.	yy,mm,dd	class	h_m (Mm)	a_m ($\mathrm{m\,s^{-2}}$)	f_m ($\mathrm{m\,s^{-2}}$)	h_0 (Mm)	ω ($10^{-3}\,\mathrm{s^{-1}}$)	ref.
1	67.02.22	FS-top	4	1383±200	1654	5	2.4±0.1	1
2	67.04.01	EP-mid	213	85±20	246	160	1.12±0.21	1
3	68.04.28	EP-mid	160	122±30	304	53	1.08±0.08	2
4	70.08.03	FS-top	21	400±100	685	6,7	4.3±0.1	3
5	71.05.03	EP-mid	205	116±40	278	190	1.1±0.5	4
6*	72.07.03	FS-top	36	764±75	1012	19	15.4±3.2	5
7*	73.02.18	FS-top	110	1470±250	1675	11	3.6±0.7	5
8*	73.06.10	CT-top	-	-	-	2100	0.38±0.09	6,7
9*	73.08.10	CT-top	-	-	-	1400	0.06±0.02	6,7
10*	73.08.21	CT-top	-	-	-	1700	0.08±0.02	6,7
11*	73.08.26	CT-top	-	-	-	1000	0.37±0.08	6,7
12*	73.09.05	FS-top	90	2230±220	2445	14	5.5±0.2	5
13*	73.09.06	CT-top	-	-	-	1550	0.39±0.05	6,7
14*	73.09.11	CT-top	-	-	-	900	1.25±0.2	6,7
15*	73.10.27	FS-top	59	920±220	1148	18	4.4±1.1	5
16*	73.12.16	CT-top	-	-	-	1100	0.05±0.01	6,7

Table 1. (continued)

No.	yy,mm,dd	class	h_m (Mm)	a_m ($\mathrm{m\,s^{-2}}$)	f_m ($\mathrm{m\,s^{-2}}$)	h_0 (Mm)	ω ($10^{-3}\,\mathrm{s^{-1}}$)	ref.
17*	73.12.19	CT-top	-	-	-	700	0.13±0.03	6,7
18*	73.12.19	EP-top	300	7.6±0.9	142	150	0.33±0.08	8
19*	73.12.19	CAV-top	2200	37±5	53	650	0.14±0.01	8
20*	74.01.15	CT-top	-	-	-	1100	0.04±0.01	6,7
21*	74.04.30	EP-top	190	320±20	492	142	1.9±0.7	5
22	79.05.07	EP-top	150	107±20	293	140	1.66±0.25	-
23*	80.02.15	CT-top	-	-	-	560	0.3±0.1	9
24*	80.08.05	CT-top	-	-	-	320	0.3±0.05	9
25	80.08.18	EP-mid	550	240±50	326	180	0.65±0.02	10,11,12,1
26	81.07.17	FS-top	12	600±300	865	3.5	7±2	-
27*	81.08.29	CT-top	-	-	-	380	1.7±0.3	9
28*	82.06.24	CT-top	-	-	-	210	0.3±0.1	9
29*	82.07.10	CT-top	-	-	-	280	0.15±0.5	9
30*	88.01.09	CAV-top	1200	6±4	43	800	0.18±0.01	-
31*	88.06.01	CAV-top	1800	19±6	40	710	0.15±0.02	-

Table 1. (continued)

No.	yy,mm,dd	class	h_m (Mm)	a_m (m s^{-2})	f_m (m s^{-2})	h_0 (Mm)	ω (10^{-3} s^{-1})	ref.
32	89.06.23	EP-mid	-	-	-	50	0.78±0.25	13
33	89.09.15	EP-mid	140	1428±40	1618	62	5.4±2.1	14
33*	92.04.04	EP-top	500	80±30	173	190	0.36±0.06	15
34*	92.04.04	CAV-top	2300	160±50	172	600	1.08±0.22	15
35*	92.05.04	EP-top	500	385±55	478	110	1.5±0.7	15
36*	93.04.30	EP-top	400	35±15	144	370	0.38±0.15	15
37*	93.04.30	CAV-top	900	100±40	152	800	1.1±0.3	15
38	94.06.29	EP-top	-	-	-	100	0.11±0.01	16
39	94.06.29	EP-top	120	20±10	220	57	0.75±0.31	16
40*	96.07.07	CT-top	4500	8.5±4.5	13	3400	0.05±0.02	17
41*	96.07.08	CT-top	1225	20±10	56	1100	0.13±0.5	17
42	98.01.21	CT-top	3500	11±3	19	-	-	-
43	98.04.23	CT-top	1700	525±45	548	-	-	-
44	98.04.27	CT-top	1500	359±42	387	-	-	-
45	98.05.02	CT-top	2200	181±31	197	-	-	-

Table 1. (continued)

No.	yy,mm,dd	class	h_m (Mm)	a_m ($\mathrm{m\,s^{-2}}$)	f_m ($\mathrm{m\,s^{-2}}$)	h_0 (Mm)	ω ($10^{-3}\,\mathrm{s^{-1}}$)	ref.
46	98.05.11	CT-top	1500	68±22	96	-	-	-
47	98.09.27	FS-top	10	1200±500	1466	5,5	20±5	-
48	99.09.03	EP-top	250	150±50	299	50	1.28±0.21	-
49	99.09.03	EP-top	100	50±20	260	-	-	-
mean		FS	43±40	1120±570	1370±570	10±6	8±6	
mean		EP	270±150	230±360	380±360	130±80	1.2±1.2	
mean		CT	2000±1000	120±160	150±160	970±740	0.44±0.49	

In the last column the references related to a given event are listed: 1 – [*Godoli et al.*, 1967]; 2 – [*Machado,* 1972]; 3 – [*Sakurai,* 1976]; 4 – [*Rybansky,* 1971]; 5 – [*Tandberg-Hanssen et al.*, 1980]; 6 – [*Gosling et al.*, 1976]; 7 – [*Anzer,* 1978]; 8 – [*Schmahl and Hildner,* 1977]; 9 – [*MacQeen and Fisher,* 1983]; 10 – [*Rušin and Rybansky,* 1982]; 11 – [*Illing and Hundhausen,* 1986]; 12 – [*Rompolt,* 1990]; 13 – [*Vršnak et al.*, 1993]; 14 – [*Rybansky and Noony,* 1990]; 15 – [*Hiei,* 1998]; 16 – [*Lenža,* 1998]; 17 – [*Dryer et al.*, 1998].

Table 2. The Occurrence Rate of Different

Kinematical Forms

form	FS	EP	CT	tot
exp.	6 (75%)	26 (87%)	14 (82%)	46 (84%)
$a = const.$	2 (25%)	3 (10%)	1 (6%)	6 (11%)
ir.	0 (0%)	1 (3%)	2 (12%)	3 (5%)
?	0	1	31	32
$a \searrow$	0 (0%)	3 (25%)	2 (7%)	5 (11%)
$v = const.$	1 (33%)	5 (42%)	19 (65%)	25 (57%)
$v \searrow$	2 (67%)	4 (33%)	8 (28%)	14 (32%)
?	5	19	19	43

Table 3. Accelerations and Growth Rates

	FS	EP	CT
$\overline{h}_{\log}$ (Mm)	${}_{8}26^{83}$	${}_{130}230^{410}$	${}_{1200}1800^{2900}$
$R/R_{\odot}$	${}_{1.01}1.04^{1.12}$	${}_{1.2}1.3^{1.6}$	${}_{2.7}3.6^{5.1}$
g ($\mathrm{m\,s^{-2}}$)	244	142	18
$\overline{a}_{\log}$ ($\mathrm{m\,s^{-2}}$)	${}_{600}1000^{1700}$	${}_{30}100^{380}$	${}_{10}50^{230}$
$\overline{f}_{\log}$ ($\mathrm{m\,s^{-2}}$)	${}_{800}1300^{1900}$	${}_{160}300^{550}$	${}_{27}85^{270}$
$\overline{h}_{0_{\log}}$ (Mm)	${}_{4.6}8.7^{16.6}$	${}_{62}112^{204}$	${}_{295}724^{1780}$
$\overline{\omega}_{\log}$ ($10^{-3}\,\mathrm{s^{-1}}$)	${}_{3.0}6.1^{12.6}$	${}_{0.34}0.85^{2.1}$	${}_{0.08}0.24^{0.75}$

The presented values are calculated from the mean (and standard deviation) of the logarithms of a given quantity (the standard deviation range is given by subscripts and superscripts).

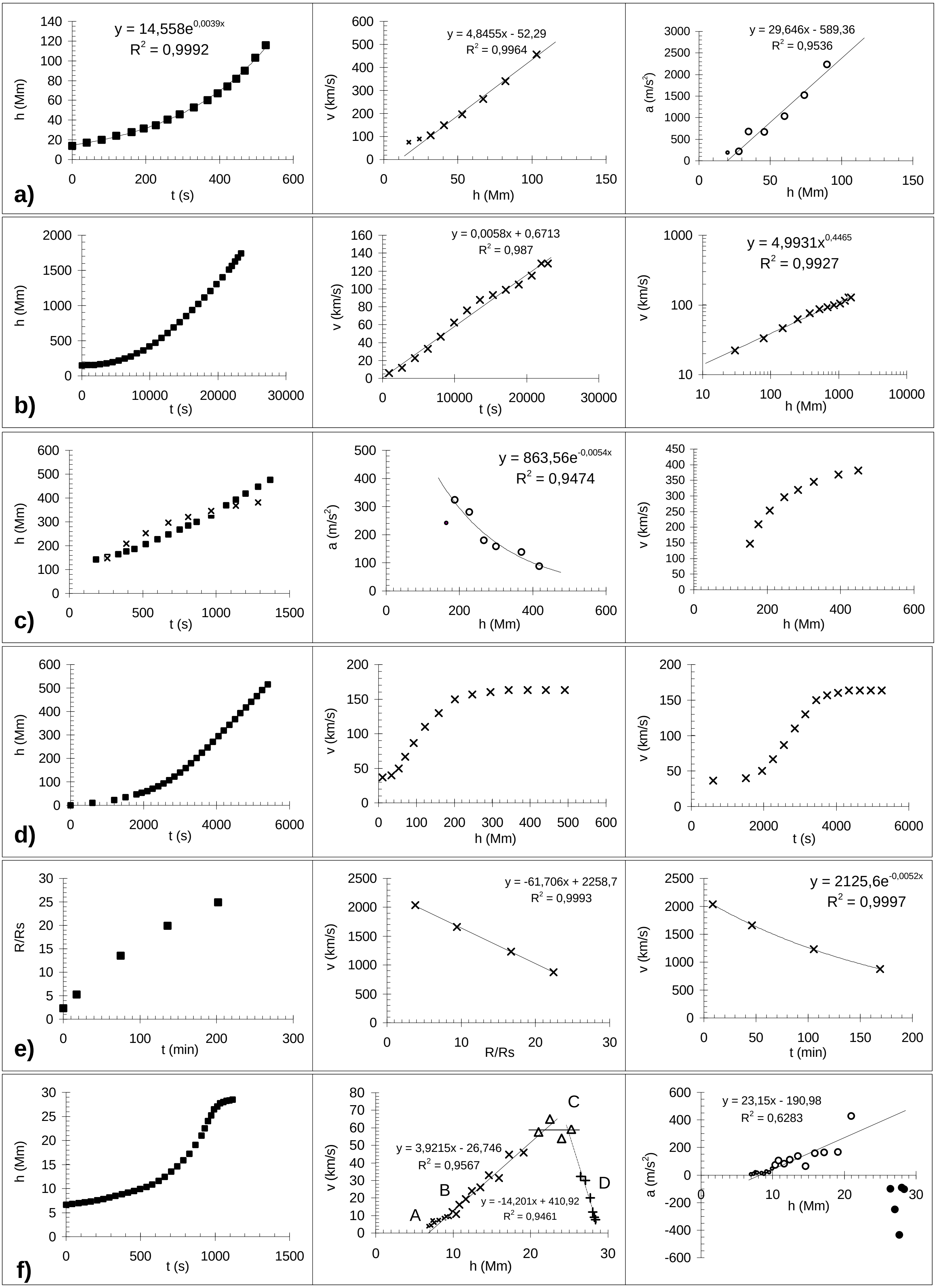

a)
h (Mm)
t (s)
y = 14,558e^0,0039x
R^2 = 0,9992
v (km/s)
h (Mm)
y = 4,8455x - 52,29
R^2 = 0,9964
a (m/s^2)
h (Mm)
y = 29,646x - 589,36
R^2 = 0,9536
b)
h (Mm)
t (s)
v (km/s)
t (s)
y = 0,0058x + 0,6713
R^2 = 0,987
v (km/s)
h (Mm)
y = 4,9931x^0,4465
R^2 = 0,9927
c)
h (Mm)
t (s)
a (m/s^2)
h (Mm)
y = 863,56e^-0,0054x
R^2 = 0,9474
v (km/s)
h (Mm)
d)
h (Mm)
t (s)
v (km/s)
h (Mm)
v (km/s)
t (s)
e)
R/Rs
t (min)
v (km/s)
R/Rs
y = -61,706x + 2258,7
R^2 = 0,9993
v (km/s)
t (min)
y = 2125,6e^-0,0052x
R^2 = 0,9997
f)
h (Mm)
t (s)
v (km/s)
h (Mm)
A
B
C
D
y = 3,9215x - 26,746
R^2 = 0,9567
y = -14,201x + 410,92
R^2 = 0,9461
a (m/s^2)
h (Mm)
y = 23,15x - 190,98
R^2 = 0,6283

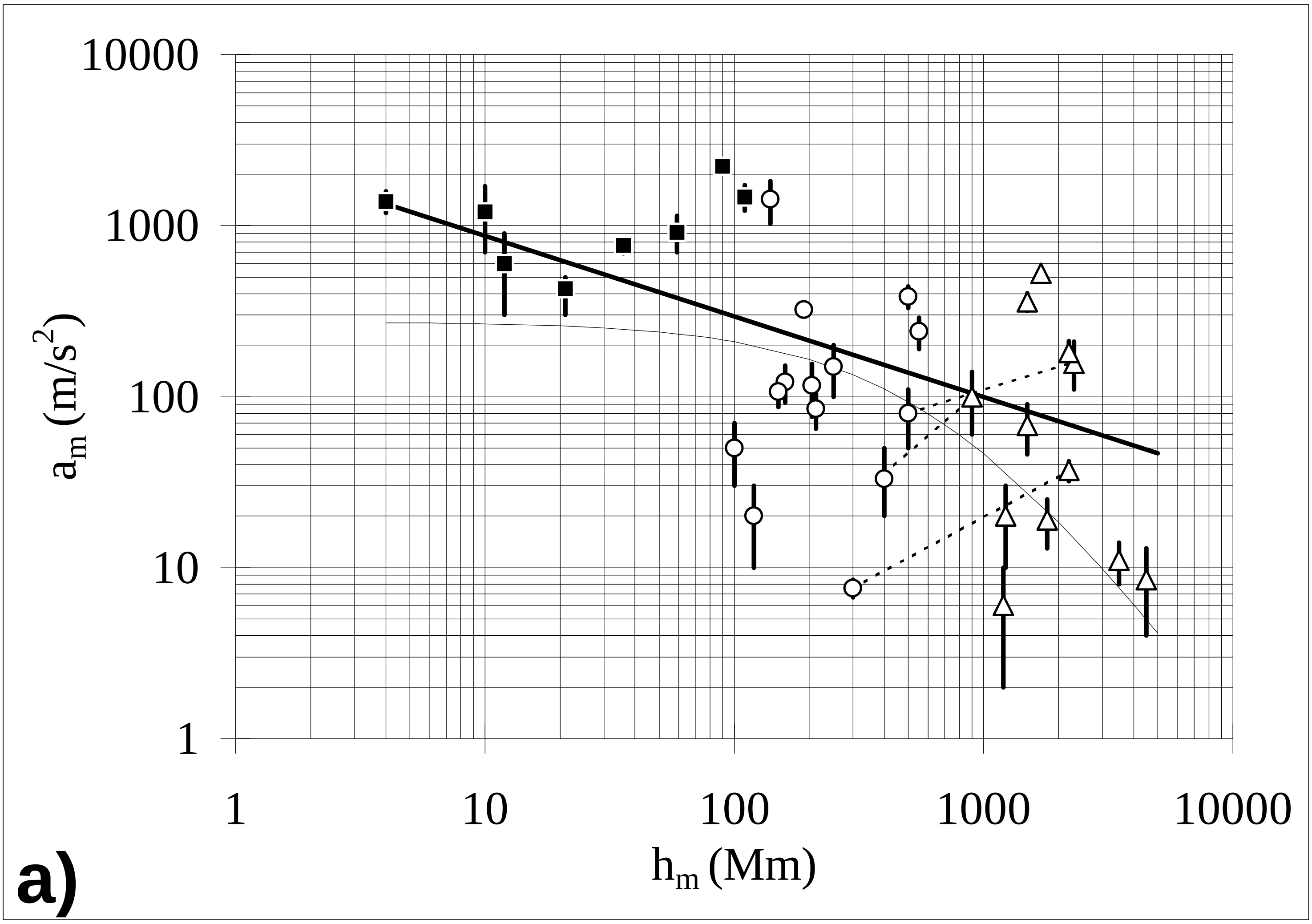

10000
1000
100
10
1
a_m (m/s^2)
1
10
100
1000
10000
h_m (Mm)
a)

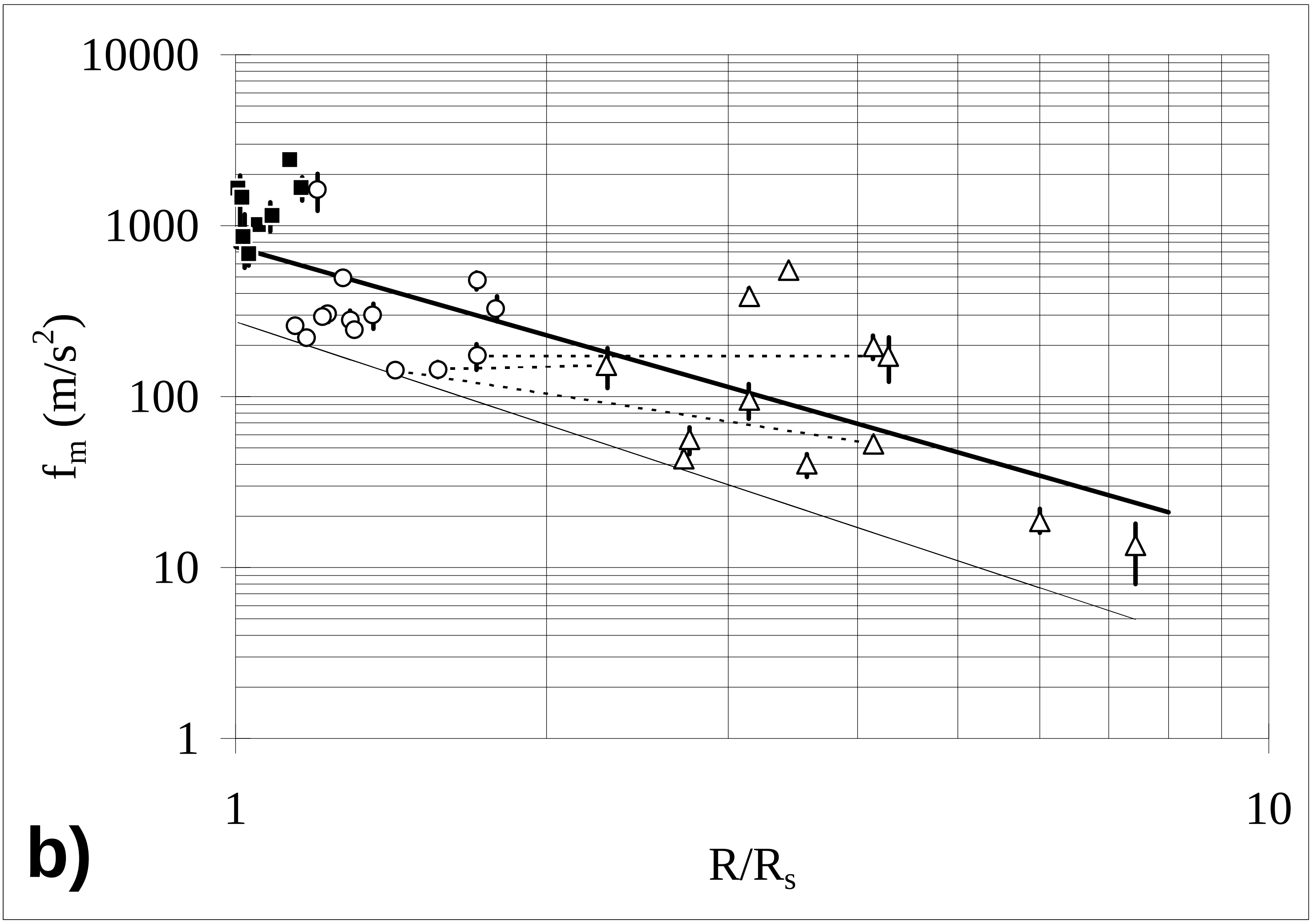

10000
1000
100
10
1
f_m (m/s^2)
1
10
R/R$_s$
b)

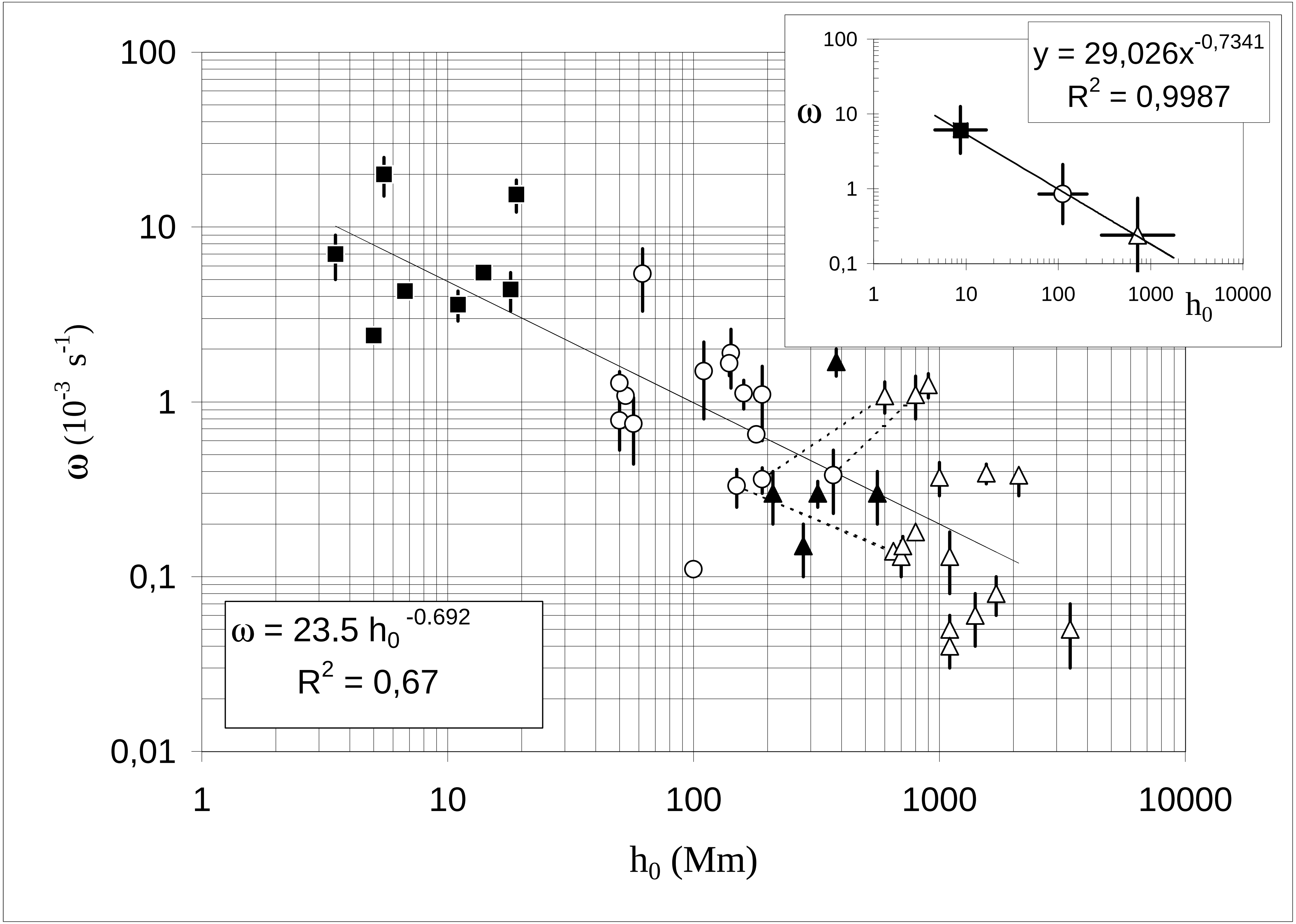

100
10
1
0,1
0,01
1
10
100
1000
10000
ω (10-3 s-1)
h0 (Mm)
ω = 23.5 h0 -0.692
R2 = 0,67
y = 29,026x-0,7341
R2 = 0,9987
ω
h0